Monitoring Therapy Response of Experimental Arthritis with Radiolabeled Tracers Targeting Fibroblasts, Macrophages, or Integrin $\alpha_v\beta_3$

Samantha Y.A. Terry[1,2], Marije I. Koenders[3], Gerben M. Franssen[1], Tapan K. Nayak[4], Anne Freimoser-Grundschober[5], Christian Klein[5], Wim J. Oyen[1], Otto C. Boerman[1], and Peter Laverman[1]

[1]Department of Radiology and Nuclear Medicine, Radboud University Medical Center, Nijmegen, The Netherlands; [2]Department of Imaging Chemistry and Biology, King's College London, London, United Kingdom; [3]Department of Experimental Rheumatology, Radboud University Medical Center, Nijmegen, The Netherlands; [4]Roche Pharmaceutical Research and Early Development, Roche Innovation Center Basel, Basel, Switzerland; and [5]Roche Innovation Center Zurich, Zurich, Switzerland

Rheumatoid arthritis is an autoimmune disease resulting in chronic synovial inflammation. Molecular imaging could be used to monitor therapy response, thus enabling tailored therapy regimens and enhancing therapeutic outcome. Here, we hypothesized that response to etanercept could be monitored by radionuclide imaging in arthritic mice. We tested 3 different targets, namely fibroblast activation protein (FAP), macrophages, and integrin $\alpha_v\beta_3$. **Methods:** Male DBA/1J mice with collagen-induced arthritis were treated with etanercept. SPECT/CT scans were acquired at 1, 24, and 48 h after injection of ^{111}In-RGD_2 (integrin $\alpha_v\beta_3$), ^{111}In-anti-F4/80-A3-1 (antimurine macrophage antibody), or ^{111}In-28H1 (anti-FAP antibody), respectively, with nonspecific controls included. Mice were dissected after the last scan, and scans were analyzed quantitatively and were correlated with macroscopic scoring. **Results:** Experimental arthritis was imaged with ^{111}In-28H1 (anti-FAP), ^{111}In-anti-F4/80-A3-1, and ^{111}In-RGD_2. Tracer uptake in joints correlated with arthritis score. Treatment decreased joint uptake of tracers from 23 ± 15, 8 ± 4, and 2 ± 1 percentage injected dose per gram (%ID/g) to 11 ± 11 ($P < 0.001$), 4 ± 4 ($P < 0.001$), and 1 ± 0.2 %ID/g ($P < 0.01$) for ^{111}In-28H1, ^{111}In-anti-F4/80-A3-1, and ^{111}In-RGD_2, respectively. Arthritis-to-blood ratios (in mice with arthritis score 2 per joint) were higher for ^{111}In-28H1 (5.5 ± 1; excluding values > 25), ^{111}In-anti-F4/80-A3-1 (10.4 ± 4), and ^{111}In-RGD_2 (7.2 ± 1) than for control ^{111}In-DP47GS (0.7 ± 0.5; $P = 0.002$), ^{111}In-rat IgG2b (0.5 ± 0.2; $P = 0.002$), or coinjection of excess RGD_2 (3.5), indicating specific uptake of all tracers in arthritic joints. **Conclusion:** ^{111}In-28H1, ^{111}In-anti-F4/80-A3-1, and ^{111}In-RGD_2 can be used to specifically monitor the response to therapy in experimental arthritis at the molecular level. Further studies, however, still need to be performed.

Key Words: experimental arthritis; fibroblast activation protein; macrophages; RGD peptide; therapy response

J Nucl Med 2016; 57:467–472
DOI: 10.2967/jnumed.115.162628

Rheumatoid arthritis is an autoimmune disease with a global prevalence of 0.24% in 2010 (*1*). Arthritis is marked by symptoms including joint pain and swelling caused by chronic inflammation in synovial joints and can be treated systemically or intraarticularly by either nonsteroidal antiinflammatory drugs, corticosteroids, or disease-modifying antirheumatic drugs (DMARDs) (*2,3*). In addition, treatment with biologicals has been shown to be quite effective in patients.

Because arthritis is a chronic disease characterized by disease exacerbations (*4*), it has become crucial to develop tools to effectively monitor disease progression, prevent progressive destruction, and predict or monitor response to therapy, which are as important for a positive outcome as early diagnosis. Monitoring response to therapy could allow for the therapeutic schedules—aimed to reduce inflammation, relieve pain, and reduce disabilities—to be altered if deemed necessary. This could thus minimize unwarranted side effects and irreversible joint damage. This is especially pertinent for therapies such as DMARDs, in which it can take several weeks to months for clinical improvements to show (*5*).

Many cell types that play a role in joint inflammation and destruction are present in the synovial lining. One of the most prominent cell populations is activated fibroblastlike synoviocytes (*6*), which express fibroblast activation protein (FAP) (*7*) and could be imaged by micro-SPECT using radiolabeled antibodies against FAP, as shown by us recently (*8*). Other cell types include osteoclasts (*9*), which express integrin $\alpha_v\beta_3$ (*10*). Integrin $\alpha_v\beta_3$ is a much-used target for imaging tumor cells and angiogenesis in oncology using radiolabeled RGD peptides. Preclinically, F4/80 receptor–positive macrophages also play a role in arthritis pathogenesis (*11*). These targets have previously been successfully imaged by either radiolabeled RGD-based peptides (*12*) or an anti-F4/80-A3-1 labeled with ^{111}In (*13*), albeit in an oncologic setting.

Noninvasive imaging could be a great tool in determining early on whether therapies are successful (*14,15*), yet few approaches have been aimed at a molecular level specific for arthritis. Here, we focused on imaging these 3 different targets, namely FAP, macrophages, and integrin $\alpha_v\beta_3$, and determined whether they could be useful tools to monitor response to the tumor necrosis factor (TNF) receptor fusion protein etanercept therapy in arthritic mice. These targets were also chosen because the treatment used here, etanercept, targets TNF, which is produced mainly by monocyte-macrophages, activated endothelial cells, which also express integrin $\alpha_v\beta_3$ (*16*), and synovial fibroblasts (*17*).

For correspondence or reprints contact: Samantha Terry, Division of Imaging Sciences and Biomedical Engineering, King's College London, St. Thomas' Hospital, London, U.K. SE1 7EH.
E-mail: samantha.terry@kcl.ac.uk
Published online Dec. 3, 2015.

MATERIALS AND METHODS

Antibody Conjugation and RGD Peptide

Rat antimouse anti-F4/80-A3-1 antibody (AbD Serotec) and rat IgG2b (R&D Systems) were dialyzed against 1:1 phosphate-buffered saline (pH 7.4):water to remove sodium azide. Antibodies 28H1 (anti-FAP), DP47GS (*8*), anti-F4/80-A3-1, and rat IgG2b (*13*) were conjugated with isothiocyanatobenzyl–diethylenetriamenepentaacetic acid (p-SCN-Bz-DTPA) (Macrocyclics, Inc.) in 0.1 M $NaHCO_3$, pH 9.5, using a 5-fold (28H1, DP47GS) or 10-fold (anti-F4/80-A3-1, IgG2b) molar excess of p-SCN-Bz-DTPA for 1 h at room temperature. Unconjugated p-SCN-Bz-DTPA was removed by dialysis against 0.25 M ammonium acetate buffer, pH 5.5 (28H1, DP47GS), or 0.1 M 2-(*N*-morpholino)ethanesulfonic acid (MES), pH 5.5 (anti-F4/80-A3-1, IgG2b). DP47GS and rat IgG2b antibodies served as isotype controls for 28H1 and anti-F4/80-A3-1, respectively.

DOTA-E-$[c(RGDfK)]_2$ (RGD_2) was acquired from Peptides International. Here we used the 28H1 and DP47GS antibodies, which are noninternalizing antibodies bearing a mutation in the Fc effector part, preventing binding to the Fc receptor. All buffers used were metal-free.

The affinity of all 3 tracers and the immunoreactive fraction of anti-F4/80-A3-1 (75%) have been determined previously (*8,13,18*). The immunoreactive fraction for ^{111}In-28H1 was 91.4% (Supplemental Fig. 1; supplemental materials are available at http://jnm.snmjournals.org).

Radiolabeling

For radiolabeling, 750 μg of DTPA-28H1 or DTPA-DP47GS were incubated with 250–320 MBq of $^{111}InCl_3$ (Mallinckrodt BV) in 0.1 MES buffer (pH 5.4) for 30 min at room temperature. For studies involving anti-F4/80-A3-1 or rat IgG2b, 280–320 MBq of $^{111}InCl_3$ (Mallinckrodt) were added to 140 μg of DTPA-anti-F4/80-A3-1 or 125 μg of rat IgG2b for 1 h at room temperature in 0.1 MES buffer (pH 5.4). For studies involving RGD_2, 8 μg of DOTA-conjugated peptide, dissolved in 0.1 M MES buffer (pH 5.4), were incubated with 200 MBq of $^{111}InCl_3$ for 20 min at 95 °C. Unincorporated ^{111}In was complexed by adding ethylenediaminetetraacetic acid (final concentration of 5 mM) after the labeling.

Labeling efficiencies of all antibodies and the RGD_2 peptide were determined by instant thin-layer chromatography on instant thin-layer chromatography silica gel strips (Agilent Technologies), with 0.1 M acetate buffer, pH 5.4, as the mobile phase. Labeling efficiencies were 93%, 99%, 91%, 95%, and 99% for ^{111}In-28H1, ^{111}In-DP47GS, ^{111}In-anti-F4/80-A3-1, ^{111}In-rat IgG2b, and ^{111}In-RGD_2, respectively. Tracers were diluted with phosphate-buffered saline (with 0.5% bovine serum albumin), and unlabeled antibody or peptide was added to obtain the required antibody or peptide dose.

Animal Model

Mice (22–25 g) were housed in individually ventilated cages, with 5 mice per cage in a temperature- and humidity-controlled room with a 12/12-h light/dark cycle. Animals had unlimited access to water and food. Arthritis was induced in male DBA/1J mice by intradermal immunization at the tail base with 100 μg of bovine type II collagen (CII) in Freund's complete adjuvant, followed by an intraperitoneal booster injection of 100 μg of CII in phosphate-buffered saline 3 wk later (collagen-induced arthritis [CIA]). Arthritis scores per paw ranged from mild to severe (score: 0, no sign of arthritis; 0.25, 1–2 toes red or swollen; 0.5, 3–5 toes red or swollen; 1, swollen ankle; 1.5, swollen footpad; 2, severe swelling and ankylosis). Etanercept treatment (10 mg/kg, 3× per week, intraperitoneally) started when the mice showed the first signs of the onset of arthritis (score ≥ 0.25 in 1 joint). Untreated arthritic mice were used as a control. Animal experiments were approved by the local animal welfare committee and performed according to national regulations.

Biodistribution Studies

In dose-finding studies, arthritic male DBA/1J mice were injected intravenously with either 10 or 40 μg of ^{111}In-anti-F4/80-A3-1 or ^{111}In-IgG2b, as done previously for ^{111}In-28H1, and the biodistribution was measured by ex vivo analysis of the accumulation of the tracer in different organs and joints after dissection of the mice. In other biodistribution studies, treated and untreated male mice were injected intravenously with 50 μg of ^{111}In-DTPA-28H1 or ^{111}In-DTPA-DP47GS, 10 μg of ^{111}In-anti-F4/80-A3-1 or ^{111}In-rat IgG2b, or 1 μg (radiolabeled) or 50 μg (1 μg + 49 μg unlabeled) of ^{111}In-RGD_2 (3–4 MBq). At 48 h (^{111}In-DTPA-28H1 and ^{111}In-DTPA-DP47GS), 24 h (^{111}In-anti-F4/80-A3-1 and ^{111}In-rat IgG2b), and 1 h (^{111}In-RGD_2) after tracer injection, mice were euthanized by CO_2/O_2 asphyxiation. Ten mice were used per group for which blood, arthritic joints, and major organs and tissues were dissected, weighed, and counted in a shielded well-type γ-counter (Perkin-Elmer) to provide the percentage injected dose per gram (%ID/g).

Micro-SPECT/CT Imaging

In imaging studies, treated and untreated male mice were injected intravenously with 50 μg of ^{111}In-DTPA-28H1 or ^{111}In-DTPA-DP47GS, 10 μg of ^{111}In-anti-F4/80-A3-1 or ^{111}In-rat IgG2b, or 1 μg (radiolabeled) or 50 μg (1 μg + 49 μg unlabeled) of ^{111}In-RGD_2 (15–21 MBq). At 48 h (^{111}In-DTPA-28H1 and ^{111}In-DTPA-DP47GS), 24 h (^{111}In-anti-F4/80-A3-1 and ^{111}In-rat IgG2b), and 1 h (^{111}In-RGD_2) after tracer injection, mice were euthanized by CO_2/O_2 asphyxiation for ex vivo biodistribution studies (3 mice/group). Mice were then scanned with the U-SPECT-II/CT scanner (MILabs) while in the prone position. Micro-SPECT scans were acquired as 3 frames of 15 min using a 1.0-mm pinhole ultrahigh-sensitivity mouse collimator, followed by a CT scan for anatomic reference (65 kV, 615 μA). Scans were reconstructed and all frames combined with software from MILabs, using an ordered-subset expectation maximization algorithm, with a voxel size of 0.4 mm. For high-resolution micro-SPECT imaging of an arthritic joint, a focal image was acquired using a 0.35-mm ultrahigh-resolution pinhole collimator at 9 frames of 18 min. Images were reconstructed to a voxel size of 0.125 mm without attenuation correction.

Quantitative SPECT Analysis

Reconstructed micro-SPECT scans were coregistered with CT images using Inveon Research Workplace software (version 3.0; Siemens Preclinical Solutions, LLC). The regions of interest were drawn using CT images and transferred to the SPECT data to obtain mean voxel intensities of the SPECT data corresponding to those regions of interest. Mean voxel intensity values were converted to %ID using decay correction and a standard curve (mean voxel intensity vs. kBq) acquired by scanning and reconstructing known ^{111}In activities from 15 to 310 kBq under the same conditions as the animal scans.

Statistical Analysis

Statistical analysis was performed using the Wilcoxon signed-rank test or 2-way ANOVA with GraphPad Prism (version 5.03; GraphPad Software). Each paw was analyzed as an independent event. Spearman r correlation values between arthritis-to-blood values and arthritis score were calculated for Figure 1. Statistical significance was represented as $P \leq 0.05$), $P \leq 0.01$, and $P \leq 0.001$.

RESULTS

Dosing Study of ^{111}In-Anti-F4/80-A3-1

The optimal dose of ^{111}In-anti-F4/80-A3-1 in mice was determined to be 10 μg; accumulation in most tissues remained largely unaltered compared with 40 μg of ^{111}In-anti-F4/80-A3-1, yet the arthritis-to-blood ratio was increased (Supplemental Fig. 2). For instance, uptake of 10 or 40 μg of ^{111}In-anti-F4/80-A3-1 in the blood equaled 1.4 ± 0.4 or 2.3 ± 0.6 %ID/g, respectively. Notably, splenic uptake was higher at 10 μg of ^{111}In-anti-F4/80-A3-1 (103.9 ± 6.4 %ID/g) than at 40 μg of ^{111}In-anti-F4/80-A3-1 (34.6 ± 4.4 %ID/g). The

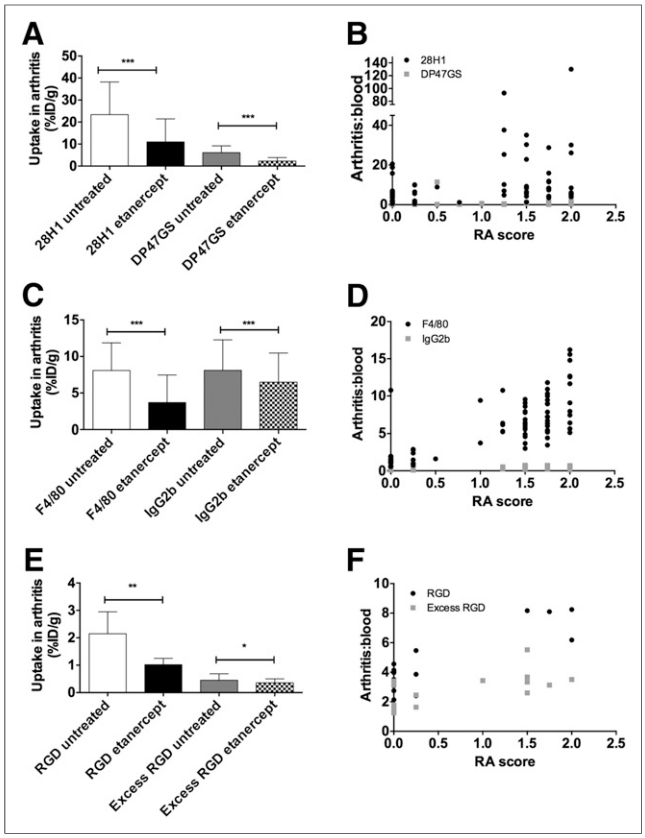

FIGURE 1. Joint uptake of tracers in untreated or etanercept-treated CIA mice at 48 h (^{111}In-28H1, ^{111}In-DP47GS; A and B), 24 h (^{111}In-anti-F4/80, ^{111}In-ratIgG2b; C and D), and 1 h after injection (^{111}In-RGD$_2$ with/without excess unlabeled; E and F). Data are average ± SD (n = 7–10 mice/group [A–D] or 2 mice/group [E and F], 4 joints per mouse [A, C, and E]) or individual joints (n = 14–20 mice/group, 4 joints per mouse; B, D, and F). *$P \leq 0.05$. **$P \leq 0.01$. ***$P \leq 0.001$. RA = rheumatoid arthritis.

arthritis-to-blood ratios were higher for 10 μg of ^{111}In-anti-F4/80-A3-1 (10.1 ± 5.2) than for 40 μg of ^{111}In-anti-F4/80-A3-1 (4.6 ± 3.2), and both values were higher than for ^{111}In-IgG2b, which equaled 0.3 ± 0.2 and 0.4 ± 0.3 at 10 and 40 μg, respectively (Supplemental Fig. 2C).

Etanercept Therapy

Treatment with etanercept was successful because macroscopic scores of arthritis were lower in treated mice than in untreated mice (Supplemental Fig. 3). At day 6 after the start of therapy, average arthritis scores were 4.0 ± 1.7 in untreated mice and 1.8 ± 1.1 in treated mice, as measured on a scale of 0–8 per mouse (i.e., 0–2 per paw).

Biodistribution Studies

Biodistribution studies after dissection showed that uptake of ^{111}In-28H1 (Spearman r, 0.4069; $P < 0.001$), ^{111}In-anti-F4/80-A3-1 (Spearman r, 0.7542; $P < 0.0001$), and ^{111}In-RGD$_2$ (Spearman r, 0.6527; $P < 0.01$) was decreased in arthritic joints in mice treated with etanercept and that tracer uptake correlated with arthritis score (Fig. 1). For instance, joint uptake of ^{111}In-28H1 in treated and untreated mice averaged 11 ± 11 %ID/g (95% confidence interval [CI], 7.0–15.1) and 23 ± 15 %ID/g (95% CI, 17.6–29.1), respectively ($P < 0.001$). Joint uptake of ^{111}In-anti-F4/80-A3-1 decreased from 8 ± 4 %ID/g (95% CI, 6.8–9.3) to 4 ± 4 %ID/g (95% CI, 2.5–4.9) after treatment ($P < 0.001$ for both tracers between treated and untreated) as did ^{111}In-RGD$_2$ uptake (from 2 ± 1 %ID/g [95% CI, 1.5–2.8] to 1 ± 0.2 %ID/g [95% CI, 0.8–1.2]) ($P = 0.0078$). Uptake of all 3 tracers when normalized to blood (arthritis-to-blood values) was higher at each arthritis score (0.25–2) for ^{111}In-28H1, ^{111}In-anti-F4/80-A3-1, and ^{111}In-RGD$_2$ than for control ^{111}In-DP47GS, ^{111}In-antiratIgG2b, and ^{111}In-RGD$_2$ plus unlabeled excess (Figs. 1B, 1D, and 1F). P values at arthritis score 2 (per joint) were 0.002, comparing ^{111}In-28H1 and ^{111}In-anti-F4/80-A3-1 with their controls.

In untreated mice, blood levels for ^{111}In-DP47GS were higher, whereas femur uptake values were lower, than for ^{111}In-28H1 (Supplemental Fig. 4A). Etanercept therapy resulted in lower blood values and higher liver values for ^{111}In-28H1 and ^{111}In-DP47GS than untreated mice (Supplemental Fig. 4A), most likely due to a mouse–antihuman IgG response. Whole-body biodistribution varied between ^{111}In-anti-F4/80-A3-1 and its isotype-matched control ^{111}In-ratIgG2b, with lower blood circulating levels and higher uptake in the spleen, liver, and femur than blood values for ^{111}In-anti-F4/80-A3-1 (Supplemental Fig. 4B). Etanercept treatment had no effect on general biodistribution of ^{111}In-anti-F4/80-A3-1, ^{111}In-ratIgG2b, ^{111}In-RGD$_2$, or ^{111}In-RGD$_2$ plus excess unlabeled (Supplemental Figs. 4B and 4C).

Table 1 shows a summary of the arthritis-to-blood values obtained in biodistribution studies.

Quantitative SPECT Analysis

Arthritic joints were specifically visualized with ^{111}In-28H1 (Fig. 2; Supplemental Fig. 5), ^{111}In-anti-F4/80-A3-1 (Fig. 3; Supplemental Fig. 6), and ^{111}In-RGD$_2$ (Fig. 4; Supplemental Fig. 7). Quantitative SPECT analysis showed that tracer uptake within joints significantly decreased in treated animals compared with untreated controls (Figs. 2–4). For instance, joint uptake equaled 2.0 ± 0.6, 0.6 ± 0.2, and 0.2 ± 0.1 %ID in untreated animals for ^{111}In-28H1, ^{111}In-anti-F4/80-A3-1, and ^{111}In-RGD$_2$, respectively. These values were higher than in treated animals (0.7 ± 0.8, 0.3 ± 0.2, and 0.08 ± 0.02 %ID). Uptake of ^{111}In-28H1 in arthritic, untreated joints was far higher (2.0 ± 0.6 %ID) than uptake of ^{111}In-DP47GS (0.8 ± 0.4 %ID), and joint uptake of ^{111}In-antiratIgG2b was not significantly decreased in untreated versus treated mice (0.7 ± 0.4 and 0.5 ± 0.4 %ID, respectively).

Values obtained for ^{111}In-28H1, ^{111}In-anti-F4/80-A3-1, and ^{111}In-RGD$_2$ by quantitative SPECT analysis correlated well with macroscopic arthritis scores (Supplemental Fig. 8).

DISCUSSION

The data acquired in the dosing study were consistent with the idea of the spleen and liver acting as an antigen sink for ^{111}In-anti-F4/80-A3-1 due to the presence of a large number of macrophages (*13*). Because of its short circulation time, studies involving ^{111}In-anti-F4/80-A3-1 were completed at 24 h after injection.

Etanercept, the drug of choice in these studies, is a soluble fusion protein consisting of human p75 TNF-α receptor and the Fc portion of human IgG (*19*). It is a biologic DMARD that inhibits binding of inflammatory cytokine TNF-α to its receptor and is often given to arthritis patients if other treatments are contraindicated or withdrawn because of adverse events.

Here, we showed that the effect of etanercept on macroscopic/clinical arthritis score can not only be visualized noninvasively using imaging tracers that target either FAP, macrophages, or integrins, but also can be measured quantitatively in either ex vivo biodistribution studies or quantitative SPECT. In previous studies,

TABLE 1
Mean and 95% CIs of Arthritis-to-Blood Uptake Ratios from Figures 1B, 1D, and 1F

Arthritis score	^{111}In-28H1	^{111}In-DP47GS (control)	^{111}In-anti-F4/80-A3-1	^{111}In-antiratIg G2b (control)	^{111}In-RGD$_2$	Cold excess RGD$_2$ (control)
0	5.0 (2.7–7.3)	0.3 (0.3–0.4)	1.8 (0.6–2.9)	0.2 (0.2–0.2)	3.5 (2.9–4.1)	2.0 (1.2–2.8)
0.25	4.8 (1.8–7.7)	0.5 (0.1–0.9)	1.7 (0.9–2.6)	0.2 (0.1–0.3)	3.9 (0.1–7.7)	2.0 (−3.2–7.3)
0.5	8.9	5.8 (−65.7–77.3)	1.6	No data	No data	No data
0.75	1.2	0.4 (−0.2–1.0)	No data	No data	No data	No data
1	No data	0.6	6.6 (−29.4–42.5)	No data	No data	3.4
1.25	11.8 (−2.9–26.6)	0.3 (0.2–0.5)	7.1 (3.2–11.1)	0.4 (0.1–0.8)	No data	No data
1.5	8.3 (1.9–14.7)	2.2 (−1.7–6.0)	6.4 (5.3–7.5)	0.5 (0.4–0.7)	8.2	3.8 (1.8–5.8)
1.75	8.4 (5.5–11.2)	0.6 (0.5–0.8)	7.6 (6.4–8.9)	0.5 (0.4–0.5)	8.1	3.1
2	5.5 (4.7–6.4)	0.7 (0.3–1.2)	10.4 (7.9–13.0)	0.5 (0.4–0.6)	7.2 (−5.9–20.3)	3.5

Where no CIs are shown, data are from $n = 1$. All values over 25 were excluded. Data in parentheses are 95% CIs.

the authors did not see accumulation of any of the tracers in the joints of nonarthritic mice (*8,12,13,18*). The 3 tracers are different with regard to their targets, mechanism, and pharmacokinetics; they all measure something different, so a straight comparison was not performed here.

The uptake of ^{111}In-28H1, ^{111}In-anti-F4/80-A3-1, and ^{111}In-RGD$_2$ is antigen/receptor-mediated because joint-to-blood values decreased for antibody controls or for ^{111}In-RGD$_2$ when competed with excess peptide (Fig. 1). For all tracers, including the RGD peptide, the enhanced permeability and retention effect did add to total tracer uptake because the nonspecific uptake of the tracer, displayed by total joint uptake values of ^{111}In-DP47GS, ^{111}In-ratIgG2b, and ^{111}In-RGD$_2$ plus excess, was altered in treated mice (Fig. 1).

Decreased antigen-mediated uptake of ^{111}In-28H1 in arthritic joints of treated CIA mice could be explained by diminished expression of FAP at the site, which fits the notion of etanercept inducing apoptosis in activated fibroblastlike synoviocytes (*20*). The potential presence of antidrug antibodies, as seen in arthritis cases for anti-TNF drugs, such as etanercept (*21,22*), human antimurine antibodies (*23*), or antihuman murine antibodies (*24*), could explain the enhanced liver uptake of ^{111}In-28H1 after etanercept treatment (Supplemental Fig. 4A). In turn, this enhanced liver uptake might also explain the lower uptake in joints of treated mice.

Decreased uptake of ^{111}In-anti-F4/80-A3-1 in arthritic joints after treatment may also be explained by lowered targeted availability because etanercept has been shown to induce apoptosis in macrophages resident in the synovium of arthritis patients at 8 wk as well as in mononuclear cells from synovial fluid in vitro (*25*). Similar targeted-mediated responses are also thought to be responsible for changes in ^{111}In-RGD$_2$ uptake in arthritic joints after etanercept therapy by affected osteoclasts (*26,27*) and vasculature (*28*). The latter option is possible, because endothelial cells have previously been targeted for use in imaging of inflammation (*29*).

Quantitative SPECT values (%ID) and biodistribution data (%ID/g) were not directly comparable in these studies, because quantitative SPECT values were derived from the whole paw (toe/finger to above ankle/wrist) and biodistribution data were derived from the areas directly surrounding the ankle/wrist. Interestingly, total non–antigen-mediated uptake of ^{111}In-ratIgG2b in the joint significantly decreased in treated compared with untreated CIA mice in biodistribution studies (Fig. 1C) yet not in the quantitative SPECT studies (Fig. 3C), likely because of a limited sensitivity of quantitative SPECT.

Because of the large variation in arthritis scores induced in the CIA mice and different responses to etanercept in individual mice, many animals had to be used per group. Despite this, the correlative figures show that these tracers can be used to objectively and quantitatively determine arthritis score in individual paws.

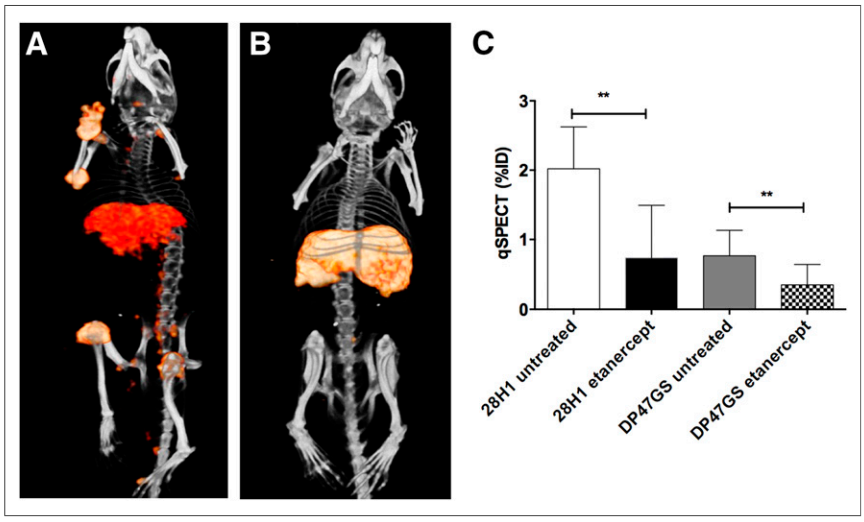

FIGURE 2. Three-dimensional SPECT/CT scans of etanercept-treated CIA mice 48 h after injection of ^{111}In-28H1 (A) and ^{111}In-DP47GS (B). All images are scaled equally. (C) Quantitative analysis of SPECT images. Data are average ± SD ($n = 3$ mice/group, 4 joints/mouse). $^{**}P \leq 0.01$.

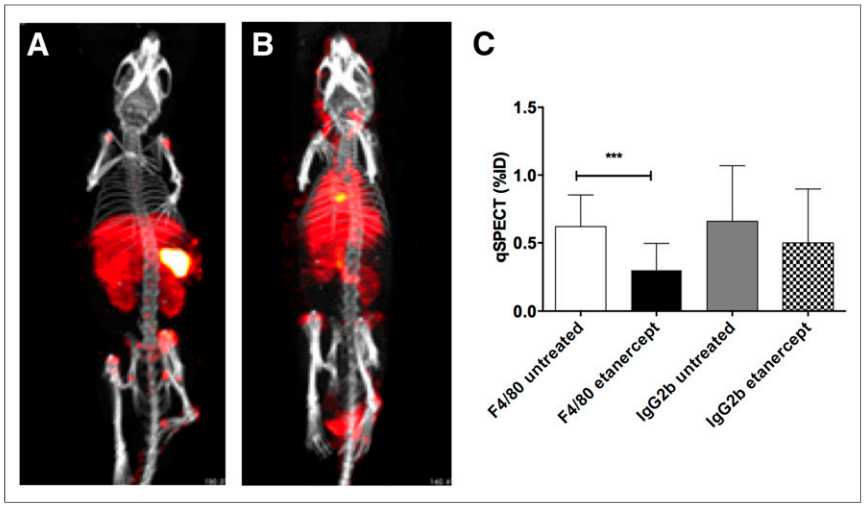

FIGURE 3. Three-dimensional SPECT/CT scans of etanercept-treated CIA mice 24 h after injection of ^{111}In-anti-F4/80 (A) and ^{111}In-ratIgG2b (B). All images are scaled equally. (C) Quantitative analysis of SPECT images. Data are average ± SD (n = 3 mice/group, 4 joints/mouse). ***$P \leq 0.001$.

Put et al. provide a review on general tracers and radiolabeled biologicals used to image inflammatory processes (*30*). Previous studies have focused mostly on targeting macrophages—either with radiolabeled folate (*31–33*), with (*R*)-^{11}C-PK11195 or translocator protein TSPO (*34–36*) (which has also been used clinically), or with radiolabeled nanobodies (*37*)—or by targeting CD163 receptors (*38*) or mannose receptors (*39*). Unfortunately, images acquired using radiolabeled folate led to poor-quality images (*31*), most probably due to general low uptake of the tracers in the joints (*32*), a feature also seen with the anti-CRIg Nanobody ^{99m}Tc-NbV4m119 (*37*). So far, the only tool to image F4/80 receptors specifically has been near-infrared-labeled antibodies (*40*), making our radiolabeled anti-F4/80-A3-1 antibody a unique nuclear tool.

Other, more generalized ways of imaging arthritis include 3′-deoxy-3′-^{18}F-fluorothymidine (*41*), which showed high background levels due to uptake in bone marrow, and ^{18}F-FDG. Despite the fact that ^{18}F-FDG was suggested as a good tool to develop the therapeutic effect of novel therapies of inflammatory arthritis in the study by Kundu-Raychaudhuri et al. (*42*), in a preclinical model Laverman et al. showed that ^{18}F-FDG was inferior to other nuclear imaging tracers when correlating uptake of ^{18}F-FDG with arthritis score (*8*).

Monitoring response to therapy in arthritis is usually performed by clinical macroscopic scoring, ultrasonography, conventional radiography, or MRI. This highlights not only the originality of the studies performed here, by targeting integrins, macrophages, or FAP in preclinical models of arthritis, but also the novelty of assessing these tracers as tools to monitor therapy response. Radionuclide-imaging-targeting-specific molecular mechanisms could therefore be a great tool alongside the standard techniques, although cost–benefit analysis will need to be performed to determine whether any potential risk from radiation dose outweighs the benefits of early and quick therapy response monitoring.

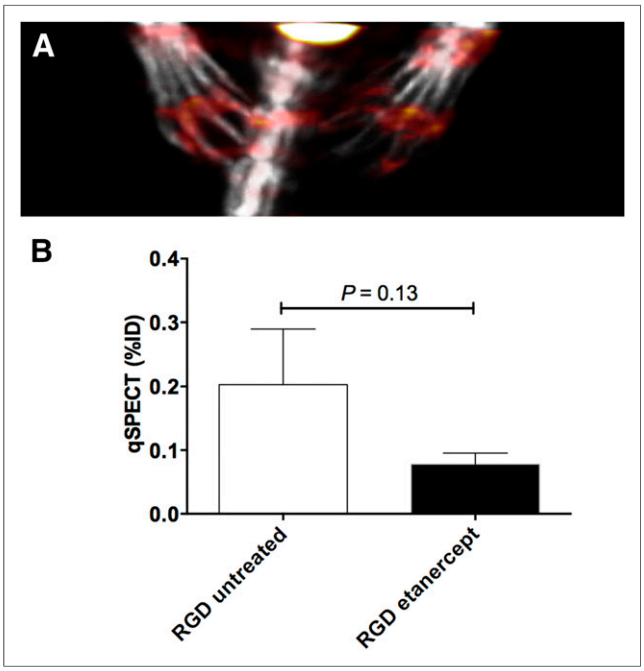

FIGURE 4. Three-dimensional SPECT/CT scans of untreated CIA mice 1 h after injection of ^{111}In-RGD$_2$ (A). (B) Quantitative analysis of SPECT images of joint uptake after injection of ^{111}In-RGD$_2$ in untreated or treated CIA mice. Data are average ± SD (n = 1–2 mice/group, 4 joints/mouse).

CONCLUSION

^{111}In-28H1, ^{111}In-anti-F4/80-A3-1, and ^{111}In-RGD$_2$ can be used to specifically monitor therapy response in experimental arthritis at the molecular level. Further studies, however, still need to be performed not only to confirm that altered target expression is the cause of the diminished uptake of all 3 tracers, but also to determine whether these tracers could be used for early diagnosis of arthritis as well as whether they can be used to monitor response to other types of therapies.

DISCLOSURE

The costs of publication of this article were defrayed in part by the payment of page charges. Therefore, and solely to indicate this fact, this article is hereby marked "advertisement" in accordance with 18 USC section 1734. A portion of this study was funded by the Roche Postdoc Fellowship (RPF) Program. Tapan K. Nayak, Anne Freimoser-Grundschober, and Christian Klein are all employed by Roche, who provided the 28H1 and DP47GS antibodies. No other potential conflict of interest relevant to this article was reported.

ACKNOWLEDGMENTS

We thank Tessa van der Geest, Danny Gerrits, and Janneke Molkenboer-Kuenen for help with the biodistribution studies.

REFERENCES

1. Cross M, Smith E, Hoy D, et al. The global burden of rheumatoid arthritis: estimates from the global burden of disease 2010 study. *Ann Rheum Dis.* 2014;73:1316–1322.

2. Rheumatoid arthritis: the management of rheumatoid arthritis in adults. NICE clinical guideline 79. National Institute for Health and Care Excellence website. https://www.nice.org.uk/guidance/cg79. Modified August 2013. Accessed January 5, 2016.
3. Firth J. Rheumatoid arthritis: treating to target with disease-modifying drugs. *Br J Nurs.* 2011;20:1240–1245.
4. Brown PM, Isaacs JD. Rheumatoid arthritis: from palliation to remission in two decades. *Clin Med.* 2014;14(suppl 6):s50–s55.
5. Dougados M, Nataf H, Steinberg G, Rouanet S, Falissard B. Relative importance of doctor-reported outcomes vs patient-reported outcomes in DMARD intensification for rheumatoid arthritis: the DUO study. *Rheumatology (Oxford).* 2013;52: 391–399.
6. Firestein GS. Invasive fibroblast-like synoviocytes in rheumatoid arthritis; passive responders or transformed aggressors? *Arthritis Rheum.* 1996;39:1781–1790.
7. Bauer S, Jendro MC, Wadle A, et al. Fibroblast activation protein is expressed by rheumatoid myofibroblast-like synoviocytes. *Arthritis Res Ther.* 2006;8:R171.
8. Laverman P, van der Geest T, Terry SY, et al. Immuno-PET and immuno-SPECT of rheumatoid arthritis with radiolabeled anti-fibroblast activation protein antibody correlates with severity of arthritis. *J Nucl Med.* 2015;56:778–783.
9. Le Goff B, Berthelot JM, Maugars Y, Heymann D. Osteoclasts in RA: diverse origins and functions. *Joint Bone Spine.* 2013;80:586–591.
10. Zheleznyak A, Wadas TJ, Sherman CD, et al. Integrin $\alpha_v\beta_3$ as a PET imaging biomarker for osteoclast number in mouse models of negative and positive osteoclast regulation. *Mol Imaging Biol.* 2012;14:500–508.
11. Bender AT, Spyvee M, Satoh T, et al. Evaluation of a candidate anti-arthritic drug using the mouse collagen antibody induced arthritis model and clinically relevant biomarkers. *Am J Transl Res.* 2013;5:92–102.
12. Terry SY, Abiraj K, Frielink C, et al. Imaging integrin $\alpha_v\beta_3$ on blood vessels with ^{111}In-RGD2 in head and neck tumor xenografts. *J Nucl Med.* 2014;55:281–286.
13. Terry SYA, Boerman OC, Gerrits D, et al. ^{111}In-anti-F4/80-A3-1 antibody: a novel tracer to image macrophages. *Eur J Nucl Med Mol Imaging.* 2015;42: 1430–1438.
14. Rosado-de-Castro PH, Lopes de Souza SA, Alexandre D, Barbosa da Fonseca LM, Gutfilen B. Rheumatoid arthritis: nuclear medicine state-of-the-art imaging. *World J Orthop.* 2014;5:312–318.
15. Tan YK, Conaghan PG. Imaging in rheumatoid arthritis. *Best Pract Res Clin Rheumatol.* 2011;25:569–584.
16. Weis SM, Cheresh DA. Tumor angiogenesis: molecular pathways and therapeutic targets. *Nat Med.* 2011;17:1359–1370.
17. McInnes IB, Schett G. Cytokines in the pathogenesis of rheumatoid arthritis. *Nat Rev Immunol.* 2007;7:429–442.
18. Dijkgraaf I, Terry SY, McBride WJ, et al. Imaging integrin alpha-v-beta-3 expression in tumors with an ^{18}F-labeled dimeric RGD peptide. *Contrast Media Mol Imaging.* 2013;8:238–245.
19. Murray KM, Dahl SL. Recombinant human tumor necrosis factor receptor (p75) Fc fusion protein (TNFR:Fc) in rheumatoid arthritis. *Ann Pharmacother.* 1997;31: 1335–1338.
20. Pattacini L, Boiardi L, Casali B, Salvarani C. Differential effects of anti-TNF-alpha drugs on fibroblast-like synoviocyte apoptosis. *Rheumatology (Oxford).* 2010;49:480–489.
21. Mok CC, van der Kleij D, Wolbink GJ. Drug levels, anti-drug antibodies, and clinical efficacy of the anti-TNFα biologics in rheumatic diseases. *Clin Rheumatol.* 2013;32:1429–1435.
22. Yi H, Kim J, Jung H, et al. Induced production of anti-etanercept antibody in collagen-induced arthritis. *Mol Med Rep.* 2014;9:2301–2308.
23. Verel I, Heider KH, Siegmund M, et al. Tumor targeting properties of monoclonal antibodies with different affinity for target antigen CD44V6 in nude mice bearing head-and-neck cancer xenografts. *Int J Cancer.* 2002;99:396–402.
24. van Gog FB, Brakenhoff RH, Snow GB, van Dongen GA. Rapid elimination of mouse/human chimeric monoclonal antibodies in nude mice. *Cancer Immunol Immunother.* 1997;44:103–111.
25. Catrina AI, Trollmo C, af Klint E, et al. Evidence that anti-tumor necrosis factor therapy with both etanercept and infliximab induces apoptosis in macrophages, but not lymphocytes, in rheumatoid arthritis joints: extended report. *Arthritis Rheum.* 2005;52:61–72.
26. Kameda H. Inhibition of the joint destruction in RA by TNF-blocking agents [article in Japanese]. *Clin Calcium.* 2007;17:553–560.
27. Yago T, Nanke Y, Kawamoto M, et al. IL-23 induces human osteoclastogenesis via IL-17 in vitro, and anti-IL-23 antibody attenuates collagen-induced arthritis in rats. *Arthritis Res Ther.* 2007;9:R96.
28. Paleolog E. Target effector role of vascular endothelium in the inflammatory response: insights from the clinical trial of anti-TNF alpha antibody in rheumatoid arthritis. *Mol Pathol.* 1997;50:225–233.
29. Jamar F, Chapman PT, Harrison AA, Binns RM, Haskard DO, Peters AM. Inflammatory arthritis: imaging of endothelial cell activation with an indium-111-labeled F(ab')2 fragment of anti-E-selectin monoclonal antibody. *Radiology.* 1995;194:843–850.
30. Put S, Westhovens R, Lahoutte T, Matthys P. Molecular imaging of rheumatoid arthritis: emerging markers, tools, and techniques. *Arthritis Res Ther.* 2014;16:208.
31. Turk MJ, Breur GJ, Widmer WR, et al. Folate-targeted imaging of activated macrophages in rats with adjuvant-induced arthritis. *Arthritis Rheum.* 2002;46: 1947–1955.
32. Gent YY, Weijers K, Molthoff CF, et al. Evaluation of the novel folate receptor ligand [^{18}F]fluoro-PEG-folate for macrophage targeting in a rat model of arthritis. *Arthritis Res Ther.* 2013;15:R37.
33. Piscaer TM, Muller C, Mindt TL, et al. Imaging of activated macrophages in experimental osteoarthritis using folate-targeted animal single-photon-emission computed tomography/computed tomography. *Arthritis Rheum.* 2011;63:1898–1907.
34. van der Laken CJ, Elzinga EH, Kropholler MA, et al. Noninvasive imaging of macrophages in rheumatoid synovitis using ^{11}C-(*R*)-PK11195 and positron emission tomography. *Arthritis Rheum.* 2008;58:3350–3355.
35. Gent YY, Voskuyl AE, Kloet RW, et al. Macrophage positron emission tomography imaging as a biomarker for preclinical rheumatoid arthritis: findings of a prospective pilot study. *Arthritis Rheum.* 2012;64:62–66.
36. Pottier G, Bernards N, Dolle F, Boisgard R. [^{18}F]DPA-714 as a biomarker for positron emission tomography imaging of rheumatoid arthritis in an animal model. *Arthritis Res Ther.* 2014;16:R69.
37. Zheng F, Put S, Bouwens L, et al. Molecular imaging with macrophage CRIg-targeting nanobodies for early and preclinical diagnosis in a mouse model of rheumatoid arthritis. *J Nucl Med.* 2014;55:824–829.
38. Eichendorff S, Svendsen P, Bender D, et al. Biodistribution and PET imaging of a novel [Ga]-anti-CD163-antibody conjugate in rats with collagen-induced arthritis and in controls. *Mol Imaging Biol.* 2015;17:87–93.
39. Put S, Schoonooghe S, Devoogdt N, et al. SPECT imaging of joint inflammation with Nanobodies targeting the macrophage mannose receptor in a mouse model for rheumatoid arthritis. *J Nucl Med.* 2013;54:807–814.
40. Hansch A, Frey O, Sauner D, et al. In vivo imaging of experimental arthritis with near-infrared fluorescence. *Arthritis Rheum.* 2004;50:961–967.
41. Fuchs K, Kohlhofer U, Quintanilla-Martinez L, et al. In vivo imaging of cell proliferation enables the detection of the extent of experimental rheumatoid arthritis by 3′-deoxy-3′-18f-fluorothymidine and small-animal PET. *J Nucl Med.* 2013;54:151–158.
42. Kundu-Raychaudhuri S, Mitra A, Datta-Mitra A, Chaudhari AJ, Raychaudhuri SP. In vivo quantification of mouse autoimmune arthritis by PET/CT. *Int J Rheum Dis.* June 26, 2014 [Epub ahead of print].